Measurement of the decay of laser-driven linear plasma wakefields

J. Jonnerby[1,†], A. von Boetticher[1], J. Holloway, L. Corner[2], A. Picksley[1,‡], A. J. Ross[1], R. J. Shalloo[3,§], C. Thornton[4], N. Bourgeois[4], R. Walczak[1,¶], S. M. Hooker[1*]

[1] *John Adams Institute for Accelerator Science and Department of Physics, University of Oxford, Denys Wilkinson Building, Keble Road, Oxford OX1 3RH, United Kingdom.*

[2] *Cockcroft Institute of Accelerator Science, Liverpool University, Liverpool, United Kingdom*

[3] *John Adams Institute for Accelerator Science, Imperial College London, London, United Kingdom*

[4] *Central Laser Facility, STFC Rutherford Appleton Laboratory, Didcot, United Kingdom*

[†] *Now at NIHR Health Protection Research Unit in Respiratory Infections, Imperial College London, London, United Kingdom*

[‡] *Now at BELLA Center, Lawrence Berkeley National Lab, Berkeley, California, United States*

[§] *Now at Deutsches Elektronen-Synchrotron DESY: Hamburg, Germany*

[¶] *Somerville College, Woodstock Road, Oxford OX2 6HD, United Kingdom*

(Dated: April 4, 2023)

We present the first measurements of the temporal decay rate of one-dimensional, linear Langmuir waves excited by an ultra-short laser pulse. Langmuir waves with relative amplitudes of approximately 6% were driven by 1.7 J, 50 fs laser pulses in hydrogen and deuterium plasmas of density $n_{e0} = 8.4 \times 10^{17}\,\mathrm{cm}^{-3}$. The wakefield lifetimes were measured to be $\tau_{\mathrm{wf}}^{\mathrm{H_2}} = (9 \pm 2)$ ps and $\tau_{\mathrm{wf}}^{\mathrm{D_2}} = (16 \pm 8)$ ps respectively for hydrogen and deuterium. The experimental results were found to be in good agreement with 2D particle-in-cell simulations. In addition to being of fundamental interest, these results are particularly relevant to the development of laser wakefield accelerators (LWFAs) and wakefield acceleration schemes using multiple pulses, such as multi-pulse laser wakefield accelerators (MP-LWFAs).

I. INTRODUCTION

Next-generation plasma wakefield particle accelerators use charged beams or laser pulses to excite Langmuir waves that can support accelerating gradients on the order of GeV/cm [1]. Considerable progress has been made in this sphere in recent years, including, for example: the acceleration to multi-GeV-scale energies in wakefields driven by laser pulses [2, 3], electron bunches [4, 5], and by long proton bunches [6]; and applications of plasma-accelerated beams to the generation of radiation [7], and the first demonstrations of gain in free-electron-laser experiments [8, 9].

In the original concept [1] of a laser-driven plasma accelerator, the driving laser pulse had a duration shorter than the plasma period $T_{pe} = 2\pi/\omega_{pe}$, where $\omega_{pe} = (Zn_{e0}e^2/m_e\epsilon_0)^{1/2}$, and in which Z is the electron number, e is the electron charge, m_e is the electron mass, and ϵ_0 is the vacuum permittivity. Many important results have been obtained in this regime, for both laser- and particle-beam-driven plasma accelerators, and this regime continues to be a major focus of research worldwide. However, it is also possible to drive the plasma wakefield with: (i) a train of short drive pulses, spaced by T_{pe}; or (ii) by a drive pulse that is long compared to T_{pe}, but with a temporal intensity profile that is modulated with a period of T_{pe} [4, 6, 10–12].

We recently extended this latter concept by proposing a new method [13] for generating the required pulse train: frequency modulation of a long laser pulse by a plasma wave driven by a short, low-energy seed pulse, followed by temporal compression in a dispersive optical system. Simulations of this scheme show that electrons could be accelerated to 0.65 GeV in a plasma stage driven by a pulse train generated by a 1.7 J, 1 ps drive pulse of the type which could be provided by a kilohertz repetition rate thin-disk laser [14]. For plasma accelerators driven by long ($\tau_{\mathrm{drive}} \gg T_{pe}$) drivers, it is important to understand the extent to which the amplitude of the plasma wave decays over the total duration of the driver.

Theoretical studies of plasma dynamics have shown that interactions between the oscillating electrons and the background ions can lead to the growth of instabilities which dissipate the Langmuir wave energy into higher-order daughter waves [15]. Ultimately, these instabilities lead to the decay of the wakefields and heating of the plasma. In this paper, we present the results of an experimental investigation of the wakefield decay rate in a parameter regime that is relevant for several current and future plasma acceleration schemes, such as plasma wakefield acceleration (PWFA) [6], laser wakefield acceleration (LWFA) [2] and multi-pulse laser wakefield acceleration (MP-LWFA) [10]. We compare our measured results with particle-in-cell simulations, and show that there is good agreement between theory, simulations, and measurements.

We first establish the key laser and plasma parameters which determine the regime in which a laser-plasma accelerator operates. When the quiver velocity of the plasma electrons in the field of the driving laser is non-relativistic, the wakefield is approximately sinusoidal,

* simon.hooker@physics.ox.ac.uk

TABLE I. Comparison of key parameters for several experiments to measure the decay of laser-driven plasma waves.

Regime	Target	Plasma	τ_L	n_{e0} / cm^{-3}	$\delta n_e/n_{e0}$	T / eV	W	τ_L/T_{pe}	$(\lambda_p/\pi\sigma)^2$	τ_{wf}/T_{pe}	τ_{wf} [ps]	Ref
LBWA	Cell	D_2	160 ps	1.07×10^{17}	0.1	20	270	623	0.11	61 ± 59	20.6 ± 20	[16]
SM-LWFA	Jet	He	400 fs	3×10^{19}	0.15	2500	4.6	20	0.023	132 ± 14	1.9 ± 0.2	[17]
SM-LWFA	Jet	He	400 fs	3.7×10^{19}	0.1	1000	5.11	21	0.033	139	1.8	[18]
SM-LWFA	Jet	H_2	400 fs	1×10^{19}	0.1	10	255	11	0.62	142 ± 28	6 ± 1	[19]
SM-LWFA	Jet	He	400 fs	1×10^{19}	0.1	10	255	11	0.62	142 ± 28	6 ± 1	[19]
LWFA	Cell	He	120 fs	1×10^{17}	0.1	14	36	0.34	31.4	33^{+33}_{-8}	8.3^{+8}_{-2}	[20]
LWFA	Jet	He	52 fs	7.4×10^{17}	0.75	13	1150	0.4	1.92	9.7	1.3	[21]
LWFA	Cell	H_2	(48.9 ± 6.3) fs	8.4×10^{17}	0.06	2	705	0.4	0.042	84 ± 25	9 ± 2	This work
LWFA	Cell	D_2	(48.9 ± 6.3) fs	8.4×10^{17}	0.04	2	262	0.4	0.042	134 ± 63	16 ± 8	This work

and is said to be in the linear regime. For a single, short driving laser pulse, this corresponds to a peak normalised vector potential $a_0 < 1$, where $a_0 = eE/m_e c\omega_0$, E the laser electric field strength, and ω_0 the laser frequency. In this regime, and for the case of a driving laser pulse with Gaussian temporal and transverse intensity profiles, the relative amplitude of the plasma wave $\delta n_e/n_{e0}$ is given by the sum of the of the relative amplitudes of the radial and longitudinal wakefields [20],

$$\begin{aligned}\frac{\delta n_e}{n_{e0}} =& \frac{\delta n_r}{n_{e0}} + \frac{\delta n_z}{n_{e0}} \\ =& A\left[\underbrace{1}_{\text{Long.}} + \underbrace{\left(\frac{2c}{\omega_{pe}\sigma}\right)^2\left(1-\frac{r^2}{\sigma^2}\right)}_{\text{Radial}}\right]\times \\ & \exp\left(\frac{-r^2}{\sigma^2}\right)\sin\left(\omega_{pe}\zeta\right) \qquad (1)\end{aligned}$$

$$A = \frac{I\sqrt{\pi}}{c^3 n_c m_e}\left(\frac{\omega_{pe}\tau_L}{2}\right)\exp\left[-\left(\frac{\omega_{pe}\tau_L}{2}\right)^2\right], \qquad (2)$$

where r is the radial distance from the propagation axis of the drive laser, ζ is the temporal delay after the peak of the drive pulse, $\omega_{pe} = (n_{e0}e^2/m_e\epsilon_0)^{1/2}$ is the plasma frequency, n_{e0} is the plasma electron density, $n_c = \epsilon_0 m_e\omega^2/e^2$ is the critical density, and ω, σ, τ_L and I are respectively the angular frequency, beam radius at the $1/e^2$ intensity, the duration (defined as the half width at $1/e^2$ intensity) and peak intensity of the driving laser pulse. The ratio of the radial to the longitudinal wakefield components at $r = 0$ is $\delta n_r/\delta n_z|_{r=0} = (2c/\omega_{pe}\sigma)^2 = (\lambda_p/\pi\sigma)^2$, where $\delta n_r/\delta n_z \gg 1$ indicates a predominantly radial wakefield and $\delta n_r/\delta n_z \ll 1$ indicates a longitudinal wakefield, which we will refer to as a one-dimensional wakefield.

The mechanisms responsible for the decay of laser-driven plasma waves have been investigated in several earlier studies. Marquès et al. [20] found that radial-dominated and longitudinal-dominated wakefields can have different decay mechanisms. Longitudinal wakefields decay through collisions [22], Landau damping [23], beam loading by accelerated particles [17], and the modulational instability [15]. The growth rate of the modulational instability is expected to be much greater than the collisional or Landau damping mechanisms, and hence will usually dominate the decay in the case when beam-loading is not significant. If the total charge trapped and accelerated by the wakefield is large, then beam loading becomes important, and can be the leading cause of the wakefield decay [17]. Radial wakefields can decay via an additional mechanism. The finite radial extent of the driving laser creates a plasma column of finite radius, and electrons with trajectories which extend outside this column will have a different oscillation period than those which remain within the plasma; this difference leads to a loss of coherence of the plasma oscillation. We expect this decay mechanism to also be important in wakefields driven in pre-formed plasma channels [24–27].

In addition to the ratio $\delta n_r/\delta n_z$, two other parameters are important in determining the mechanisms responsible for, and the rate of, wakefield decay. First, the ratio of the energy density of the Langmuir wave to the thermal energy density, $W = (v_L/v_t)^2 = \epsilon_0|\mathbf{E}|^2/2n_{e0}k_B T_e$, where $v_L = eE_L/m_e\omega_{pe}$, $v_t = (k_B T_e/m_e)^{1/2}$, E is the electric field strength of the wakefield, k_B is the Boltzmann constant, and T_e is the electron plasma temperature [15]. The parameter W determines the growth rate of the modulational instability and delineates the strong-field regime ($W \gg 1$) from the weak-field regime ($W \lesssim 1$). Second, the ratio of the drive pulse length to the plasma ion period τ_L/T_{pi}, where $T_{pi} = 2\pi/\omega_{pi}$, where $\omega_{pi} = (Zn_{e0}e^2/M\epsilon_0)^{1/2}$, and in which Z and M are the charge and mass of the ions respectively. For $\tau_L \gg T_{pi}$ the plasma instabilities driven by ion dynamics co-evolve with the drive laser, and for $\tau_L \ll T_{pi}$ they develop only after the wakefield is excited.

Table I summarises the results of previous measurements of the decay time of laser-driven wakefields. The penultimate and antepenultimate columns of the table give the time to wakefield decay τ_{wf} and the ratio of this to the electron plasma period T_{pe}. It should be noted that the precise definition of τ_{wf} varies between the experiments. In Refs. [16, 19] it refers to the total

length of the detectable wakefield signal, whereas in Refs. [17, 18, 20, 21], and in the present work, it refers to the time taken for the wakefield amplitude to decay to a level of $1/e$ of the maximum amplitude. We also note that the time given in Ref [16] refers to the saturation time of the beatwave-driven wakefield, and, for simplicity, we have taken this to be equal to the decay time. It is striking that in this prior work that, with the exception of Ref. [21], the ratio of the wakefield lifetime to the electron plasma period τ_{wf}/T_{pe} varies by less than a factor of 5 in experiments for which the plasma density and the duration of the drive pulse both vary by more than two orders of magnitude.

The earlier work summarised in Table I was undertaken in a wide range of laser-plasma accelerator regimes. In the experiment by Moulin et al. [16] a wakefield was excited using the 'beatwave' (LBWA) scheme in which two long pulses (160 ps and 90 ps), of angular frequencies ω_1 and ω_2, interfere to generate a beat pattern at the plasma frequency $\omega_{pe} = \omega_1 - \omega_2$. In that work plasma instabilities therefore developed during the excitation of the wakefield by the drive beam or drivers. The experiments by Leblanc et al. [17], Chen et al. [18], and Ting et al. [19] corresponded to the self-modulated laser wakefield (SM-LWFA) regime in which interaction between a long laser pulse ($\tau_L \gg T_{pe}$) and the weak plasma wave it drives causes the laser pulse to become modulated with a period of T_{pe}, leading to a nonlinear feedback in which the modulation of the laser pulse and the wakefield amplitude both increase with delay relative to the front of the driving pulse. Hence these experiments correspond to an intermediate regime in which the duration of the drive pulse lies between the electron plasma period and the ion plasma period T_{pi}. Finally, Marquès et al. [20] and Kotaki et al. [21] performed experiments in the LWFA regime originally proposed by Tajima and Dawson, in which the wakefield is excited by a laser pulse with $\tau_L < T_{pe}$. These last two experiments both operated in the radial-dominated wakefield regime, and shorter decay times relative to the plasma period were observed compared to the experiments that generated longitudinal-dominated wakefields. With the exception of the work by Kotaki et al. [21], in all the experiments $\delta n_e/n_{e0} \approx 0.1$, i.e. they were all conducted in the linear wakefield regime. It is noteworthy that for the much stronger wakefields ($\delta n_e/n_{e0} \approx 0.75$) studied in [21], the observed ratio τ_{wf}/T_{pe} is much smaller than found in experiments operating in the linear regime.

Before concluding this short review of prior experimental work, we note that wakefield decay and ion motion has also been studied for proton-beam-driven wakefield accelerators [28]; these results have not been included in Table I owing to the very different driver and plasma parameters. We also note recent experiments to establish the limits to the repetition rate of PWFAs driven by electron bunches [29]. The topic of the present paper, the time-scale for wakefield decay, is related to the maximum possible repetition rate of a plasma accelerator. However, we emphasize that wakefield decay is just the first step in a complex chain of processes – that includes wakefield decay, electron-ion recombination, and heat redistribution — that must be completed before the following drive pulse can be delivered.

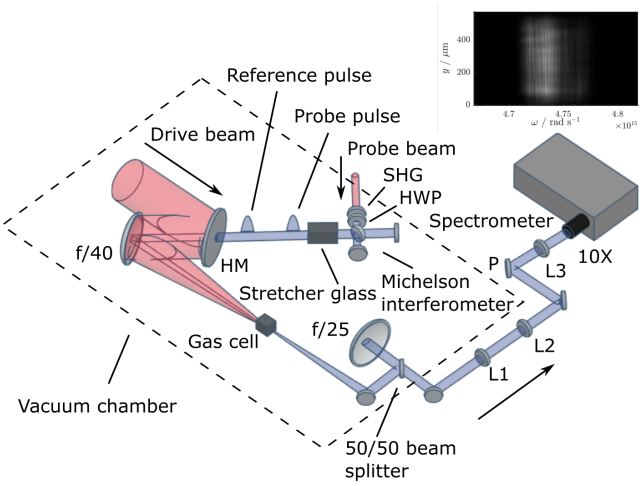

FIG. 1. Schematic drawing of the experimental layout inside the target vacuum chamber. Both beams of the Astra-Gemini TA3 laser were used: one as the drive beam, and the other as the diagnostic probe beam. The 800 nm beams are shown in red and the 400 nm diagnostic beam is shown in blue. After leaving the gas cell, the diagnostic beam was transported to a 400 nm spectrometer located outside the vacuum chamber. The inset shows an example recording of a wakefield in a spectral interferogram, as captured by the spectrometer camera. HM: Holed mirror, HWP: Half-wave plate, L1: f=500 mm lens, L2: f=−100 mm lens, L3: f=300 mm lens, P: polariser, 10X: microscope objective, SHG: second harmonic generating crystal.

To our knowledge, the new work presented in the present paper is the first measurement of the decay rate of a one-dimensional ($\delta n_r/\delta n_z \ll 1$), linear wakefield ($a_0 \sim 0.5$) in the short-pulse LWFA regime ($\tau_L/T_{pe} \approx 0.4$). This short-pulse regime is relevant for future plasma wakefield facilities [30–32] (although we note that some of these are expected to operate in the quasi-linear regime ($a_0 \sim 1$ for a single pulse) e.g. [30]), and it is also relevant to alternative schemes, such as MP-LWFAs [10, 11, 13].

II. MEASUREMENT OF THE WAKEFIELD LIFETIME

Experiments to measure the lifetime of a plasma wakefield in the 1D, linear regime were undertaken at the Central Laser Facility of the Rutherford Appleton Laboratory, using the Astra-Gemini TA3 laser. A schematic illustration of the experiment layout is shown in Fig. 1.

A linearly polarised laser pulse with energy $E = (1.68 \pm 0.06)$ J, centre wavelength 800 nm, and FWHM pulse duration (48.9 ± 6.3) fs was used to drive the wake-

field. This pulse was focused by an on-axis reflecting paraboloid of focal length $f \approx 6.1\,\mathrm{m}$, used at $f/40$, to a spot size ($1/e^2$ intensity radius) of $w_0 = (52.3 \pm 0.8)\,\mu\mathrm{m}$ at the centre of a gas cell. The peak intensity at the laser focus was $I = 6.5 \times 10^{17}\,\mathrm{W\,cm^{-2}}$, corresponding to a peak normalised vector potential of $a_0 = 0.54 \pm 0.18$, with approximately a factor of 0.3 of the beam energy enclosed within the FWHM beam diameter at focus.

Laser radiation could enter and leave the cell via a pair of coaxial, 400 µm diameter pinholes located at each end of the 4 mm long gas cell. Gas, either hydrogen (H_2) or deuterium (D_2), was flowed into the cell in a pulse of duration of approximately 500 ms; the gas flowed into the surrounding vacuum chamber via the pinholes. For these experiments the cell backing pressure was $P_{\mathrm{cell}} = (17.0 \pm 1.2)\,\mathrm{mbar}$, corresponding to an electron density $8.4 \times 10^{17}\,\mathrm{cm^{-3}}$ (assuming 100% ionization).

The amplitude of the plasma wave was measured by frequency domain holography (FDH) [33], analysed with the TESS technique [34, 35]. In this method, two chirped and stretched diagnostic pulses are generated: (i) a probe pulse, which propagates behind the drive pulse, and acquires a temporally-dependent phase shift from the density modulation of the plasma wave; and (ii) a near-identical reference pulse, which propagates ahead of the drive pulse. This pair of diagnostic pulses was generated by passing a frequency-doubled pick-off from the probe beam through a Michelson interferometer with a path difference corresponding to $\Delta\zeta \approx 6\,\mathrm{ps}$. Each of the pair of pulses thereby created was then frequency-chirped and stretched to a duration of 1.35 ps by propagating them through a 160 mm long piece of glass (BK7). The diagnostic pulses were injected coaxially with the drive beam by directing them through a holed turning mirror, and focused into the gas cell by the same optic used to focus the drive beam. On leaving the gas cell the diagnostic pulses were separated from the transmitted drive pulse by reflection from a dichroic mirror and imaged onto the entrance slit of a Czerny-Turner spectrometer to yield a spectral interferogram which was recorded by a CCD camera (Andor Newton DU940N-BU). The wakefield amplitude was calculated from the captured interferograms using the TESS technique, as follows. Each spectral interferogram was Fourier transformed along its spectral axis to give a spatio-temporal profile. The Fourier-transformed data comprises a zero-frequency ("DC") band; a sideband located at $t = \Delta\zeta$; and three satellites — two either side of the sideband, and a third located near the DC band. These satellites arise from the phase-shift imposed on the probe beam by the sinusoidal plasma wave. The satellites are offset from the sideband and have temporal locations given by [34, 35],

$$\tau = \Delta\zeta \pm \varphi^{(2)}\omega_{pe}, \tag{3}$$

where $\varphi^{(2)}$ is the group delay dispersion (GDD) of the probe and reference pulses. For plasma waves with large amplitudes, higher-order satellites can appear, located at $\tau = \Delta\zeta \pm m\varphi^{(2)}\omega_{pe}$, $m = 2, 3, 4, ...$, but these higher-order satellites were not observed in this experiment. The relative amplitude of the wakefield at delay ζ can be found from the ratio r of the satellite amplitude to that of the sideband since this is given by,

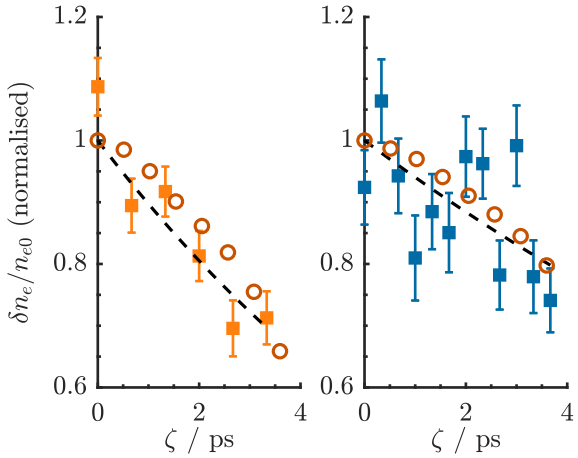

FIG. 2. Measured normalised relative wakefield amplitude as a function of delay for: (a) hydrogen; (b) deuterium, recorded with a backing pressure $P_{\mathrm{cell}} = (17.0 \pm 1.2)\,\mathrm{mbar}$. For each delay are shown the uncertainty-weighted average wakefield amplitude ($\delta n_e(\zeta)/n_{e0}$) and the standard error. The uncertainty was calculated using the background noise in the Fourier transformed interferograms. The wakefield amplitude calculated from the PIC simulations are shown as open circles. Also shown are fits of the exponential function to the data as black lines.

$$r = \mathcal{F}(\omega_{pe})\frac{J_1(\phi_0)}{J_0(\phi_0)} \tag{4}$$

where,

$$\phi_0 = \frac{\omega_{pe}^2 L}{2\omega_{\mathrm{probe}} c}\frac{\delta n_e}{n_{e0}}. \tag{5}$$

and where J_0 and J_1 are Bessel functions of the first kind, $\mathcal{F}(\omega_{pe})$ a spectral overlap function (see Supplemental Material), L is the interaction length, and ω_{probe} is the frequency of the probe laser [34, 35]. By varying the backing pressure, and measuring ω_{pe} immediately after the drive pulse, it was found that the pressure in the cell was linearly related to the measured backing pressure through $P_{\mathrm{cell}} = \alpha(P_{\mathrm{gauge}} - P_0)$, where $\alpha = 0.96$ accounts for the fact that the pressure guage was located prior to the gas cell gas inlet and $P_0 = 3$ a calibration factor (see Supplemental Material).

III. RESULTS

The wakefield amplitude was measured for a range of delays ζ in steps of 0.5 ps. For each temporal delay, the results of 10 shots were averaged in order to reduce the statistical error in the measured wake amplitude.

Figure 2 shows, for hydrogen and deuterium, the measured wakefield amplitude as a function of delay, normalised to $\delta n_e(0)$, where $\delta n_e(0)$ is determined by a fit of the function $\delta n_e(\zeta) = \delta n_e(0)\exp(-\zeta/\tau_{wf})$ to the data. Due to variations in the experimental conditions, the plasma waves driven in deuterium had an initially lower amplitude, which made the error bars relatively larger after normalisation.

Also shown in Fig. 2 are the results of 2D particle-in-cell (PIC) simulations performed with the relativistic particle-in-cell code `smilei` [Simulation of Matter Irradiated by Light at Extreme Intensities, 36] for the laser and plasma parameters used in the experiment (see Supplemental Material). The wakefield amplitude was calculated from the maximum Fourier amplitude (near ω_{pe}) of the density variation $\delta n(x,y) = \delta n_e(x,y) - \delta n_i(x,y)$ corresponding to the wakefield plasma oscillation, where $\delta n_i(x,y)$ is the ion density. The Fourier amplitude, A_F, was converted to the wakefield amplitude, $A_{\rm wake}$ using the relation $A_{\rm wake} = 2A_F\Delta x/[\int W_T^\beta(x)\,dx]$. Here $W_T^\beta(x)$ is a Tukey window with window parameter β (set to β=0.2), and $\Delta x = 26.7$ nm, the simulation cell size in the dimension along the laser axis of propagation.

The results of the simulations are seen to be in very good agreement with the experimental data. As well as correctly reproducing the timescale of the wakefield decay, the wakefield amplitudes calculated by the simulations are found to be close in absolute terms to the measured values. For both hydrogen and deuterium plasmas the relative wake amplitude at $\zeta = 0$ was calculated to be 7.5% for the laser and plasma conditions of the experiment. This compares with the measured values of (6 ± 2)% for hydrogen and (4 ± 2)% for deuterium. This agreement, which is within a factor of two, is remarkably good when it is considered that: (i) the simulations contained no free parameters; and (ii) the measured wakefield amplitude is rather sensitive to variations in many of the experimental parameters. These experimental parameters include: the pulse energy, duration, and focal spot quality of the laser pulse; the spectrum of the probe pulse; the relative alignment of the drive and diagnostic pulses; and the pressure in the gas cell.

Table II summarises the results of the measurements and simulations; to enable a comparison with the experiments, the temporal variation of the wake amplitude found in the simulations was fitted to an exponential decay. For the conditions of the experiment we find: for hydrogen, $\tau_{\rm wf} \approx 9$ ps, corresponding to around 76 plasma periods; for deuterium these values are approximately 16 ps and 134 periods respectively.

The measured wakefield lifetimes are long compared to the electron plasma period $T_{\rm pe} = 121$ fs, and are comparable to the ion plasma periods $T_{pi} = 5.2$ ps and 7.4 ps for hydrogen and deuterium respectively. The ratios of the decay times measured for deuterium and hydrogen are found to be $\tau_{wf}^{D_2}/\tau_{wf}^{H_2} = 1.76 \pm 0.95$ and 1.75 ± 0.22 from the measurements and simulations respectively. These ratios are consistent with the ratio of the inverse ion frequencies, i.e. $\omega_D^{-1}/\omega_H^{-1} = \sqrt{M_D/M_H} = \sqrt{2}$, but the error in the experimentally determined ratio is too large for it to be concluded from these measurements that τ_D/τ_H differs from unity. The value for this ratio deduced from the simulations is not consistent with unity, and is close to $\sqrt{2}$.

TABLE II. Comparison of the wakefield decay times (in picoseconds) obtained from experiments and PIC simulations.

	$\tau_{\rm wf}^{\rm H_2}$	$\tau_{\rm wf}^{\rm D_2}$	$\tau_{wf}^{D_2}/\tau_{wf}^{H_2}$
Experiment	9 ± 2	16 ± 8	1.76 ± 0.95
Simulation	8.5 ± 0.9	15 ± 1	1.75 ± 0.22

A detailed analysis of the PIC simulations [37], and comparison with work by Sanmartin et al [38], shows plasma waves in these experiments decay via the modulational instability. This instability causes small spatial variations in the ion density to grow exponentially, with a time-scale of approximately T_{pi}, leading to a loss of coherence of the electron oscillations, and hence decay of the wakefield amplitude.

IV. CONCLUSION

In conclusion, we have used single-shot frequency domain holography to measure the lifetime of 1D linear plasma wakefields in hydrogen and deuterium plasmas driven in the short-pulse LWFA regime. Wakefields with relative amplitudes of approximately 6% were driven by 1.7 J, 50 fs laser pulses in hydrogen and deuterium plasmas of density $n_{e0} = 8.4 \times 10^{17}\,{\rm cm}^{-3}$. The wakefield lifetimes were measured to be $\tau_{\rm wf}^{\rm H_2} = (9 \pm 2)$ ps and $\tau_{\rm wf}^{\rm D_2} = (16 \pm 8)$ ps respectively for hydrogen and deuterium. The experimental results were found to be in good agreement with 2D particle-in-cell simulations.

These findings are of relevance to the MP-LWFA scheme, in which the wakefield is driven resonantly by a train of short pulses [10, 11]. This latter approach is of considerable interest since it offers a route to driving LWFAs at high pulse repetition rates with novel laser technologies which can provide the required average power, with high wall-plug efficiency, but which deliver pulses which are too long to drive a plasma wave directly. The wakefield lifetime is of key importance to the MP-LWFA scheme since it determines the maximum useful number of pulses in the pulse train. The work presented here shows that, for plasma densities relevant to MP-LWFAs, the wakefield lifetime corresponds to of order 100 plasma periods, which is large compared to the $N \approx 10$ pulses required for MP-LWFA schemes [13].

V. ACKNOWLEDGEMENTS

This work was supported by the UK Science and Technology Facilities Council (STFC UK) [grant numbers ST/N504233/1, ST/P002048/1, ST/R505006/1, ST/S505833/1, ST/V001655/1]; the Engineering and Physical Sciences Research Council [EP/N509711/1, EP/V006797/1], and the Central Laser Facility. This material is based upon work supported by the Air Force Office of Scientific Research under award number FA9550-18-1-7005. This work was supported by the European Union's Horizon 2020 research and innovation programme under grant agreements No. 653782 and 730871.

[1] T. Tajima and J. M. Dawson, Phys. Rev. Lett. **43**, 267 (1979).
[2] W. P. Leemans, B. Nagler, A. J. Gonsalves, C. Tóth, K. Nakamura, C. G. R. Geddes, E. Esarey, C. B. Schroeder, and S. M. Hooker, Nature Physics **2**, 696 (2006).
[3] A. J. Gonsalves, K. Nakamura, J. Daniels, C. Benedetti, C. Pieronek, T. C. H. D. Raadt, S. Steinke, J. H. Bin, S. S. Bulanov, J. V. Tilborg, C. G. R. Geddes, C. B. Schroeder, C. Tóth, E. Esarey, K. Swanson, G. Bagdasarov, N. Bobrova, V. Gasilov, G. Korn, P. Sasorov, and W. P. Leemans, Physical Review Letters **122**, 84801 (2019).
[4] V. Yakimenko, L. Alsberg, E. Bong, G. Bouchard, C. Clarke, C. Emma, S. Green, C. Hast, M. J. Hogan, J. Seabury, N. Lipkowitz, B. O'Shea, D. Storey, G. White, and G. Yocky, Physical Review Accelerators and Beams **22**, 101301 (2019).
[5] R. Pompili, D. Alesini, M. P. Anania, M. Behtouei, M. Bellaveglia, A. Biagioni, F. G. Bisesto, M. Cesarini, E. Chiadroni, A. Cianchi, G. Costa, M. Croia, A. Del Dotto, D. Di Giovenale, M. Diomede, F. Dipace, M. Ferrario, A. Giribono, V. Lollo, L. Magnisi, M. Marongiu, A. Mostacci, L. Piersanti, G. Di Pirro, S. Romeo, A. R. Rossi, J. Scifo, V. Shpakov, C. Vaccarezza, F. Villa, and A. Zigler, Nature Physics **17**, 499 (2021).
[6] E. Adli, A. Ahuja, O. Apsimon, R. Apsimon, D. Barrientos, F. Batsch, J. Bauche, M. Bernardini, T. Bohl, C. Bracco, G. Burt, A. Caldwell, M. Cascella, J. Chappell, E. Chevallay, M. Chung, D. Cooke, H. Damerau, L. Deacon, L. H. Deubner, A. Dexter, S. Doebert, R. Fiorito, R. A. Fonseca, F. Friebel, L. Garolfi, S. Gessner, I. Gorgisyan, A. A. Gorn, J. Farmer, E. Granados, O. Grulke, E. Gschwendtner, J. Hansen, A. Helm, J. R. Henderson, M. Ibison, L. Jensen, L. M. Brun, M. Martyanov, S. Jolly, F. Keeble, F. Kraus, Y. Li, S. Liu, N. Lopes, J. Mitchell, J. C. Molendijk, J. T. Moody, M. Moreira, S. Mazzoni, D. M. Godoy, C. Pasquino, A. Pardons, K. Pepitone, A. Perera, A. Petrenko, S. Pitman, A. Pukhov, S. Rey, L. O. Silva, L. Soby, R. Speroni, K. Rieger, H. Ruhl, J. S. Schmidt, I. A. Shalimova, M. Turner, F. Velotti, L. Verra, J. Vieira, B. Williamson, R. I. Spitsyn, M. Wing, B. Woolley, and G. Xia, Nature **561**, 4 (2018).
[7] F. Albert, N. Lemos, J. L. Shaw, B. B. Pollock, C. Goyon, W. Schumaker, A. M. Saunders, K. A. Marsh, A. Pak, J. E. Ralph, J. L. Martins, L. D. Amorim, R. W. Falcone, S. H. Glenzer, J. D. Moody, and C. Joshi, Physical Review Letters **118** (2017), 10.1103/PhysRevLett.118.134801.
[8] W. Wang, K. Feng, L. Ke, C. Yu, Y. Xu, R. Qi, Y. Chen, Z. Qin, Z. Zhang, M. Fang, J. Liu, K. Jiang, H. Wang, C. Wang, X. Yang, F. Wu, Y. Leng, J. Liu, R. Li, and Z. Xu, Nature **595**, 516 (2021).
[9] M. Ferrario, Nature **605**, 659 (2022).
[10] S. M. Hooker, R. Bartolini, S. P. D. Mangles, A. Tünnermann, L. Corner, J. Limpert, A. Seryi, and R. Walczak, Journal of Physics B: Atomic, Molecular and Optical Physics **47**, 234003 (2014).
[11] J. Cowley, C. Thornton, C. Arran, R. J. Shalloo, L. Corner, G. Cheung, N. H. Matlis, D. R. Symes, R. Walczak, and S. M. Hooker, Physical Review Letters **119** (2017), 10.1103/PhysRevLett.119.044802.
[12] P. Muggli, B. Allen, V. E. Yakimenko, J. Park, M. Babzien, K. P. Kusche, and W. D. Kimura, Physical Review Special Topics - Accelerators and Beams **13**, 1 (2010).
[13] O. Jakobsson, S. M. Hooker, and R. Walczak, Phys. Rev. Lett. **127**, 184801 (2021).
[14] A. Tünnermann, T. Schreiber, and J. Limpert, Applied Optics **49**, 71 (2010).
[15] P. Mora, D. Pesme, A. Heron, G. Laval, and N. Silvestre, Physical Review Letters **61**, 1611 (1988).
[16] F. Moulin, F. Amiranoff, M. Laberge, J. R. Marquès, B. Cros, G. Matthieussent, D. Bernard, F. Jacquet, P. Miné, A. Specka, C. Stenz, and P. Mora, Physics of Plasmas **1**, 1318 (1994).
[17] S. P. L. Blanc, M. C. Downer, R. Wagner, S. Chen, A. Maksimchuk, G. Mourou, and D. Umstadter, Physical Review Letters **77**, 5381 (1996).
[18] S. Y. Chen, M. Krishnan, A. Maksimchuk, and D. Umstadter, Physics of Plasmas **7**, 403 (2000).
[19] A. Ting, K. Krushelnick, C. I. Moore, H. R. Burris, E. Esarey, J. Krall, and P. Sprangle, Physical Review Letters , 5377 (1996).
[20] J. R. Marques, F. Dorchies, F. Amiranoff, P. Audebert, J. C. Gauthier, J. P. Geindre, A. Antonetti, J. T. M. Antonsen, P. Chessa, and P. Mora, Physics of Plasmas **1162** (1997), 10.1063/1.873001.
[21] H. Kotaki, M. Kando, T. Oketa, S. Masuda, J. K. Koga, S. Kondo, S. Kanazawa, T. Yokoyama, T. Matoba, and K. Nakajima, Physics of Plasmas **9**, 1392 (2002).
[22] J. W. Banks, S. Brunner, R. L. Berger, and T. M. Tran, Physics of Plasmas **23** (2016), 10.1063/1.4943194, 1601.01002.
[23] P. M. Bellan, Fundamentals of plasma physics (Cambridge University Press, 2006).
[24] R. Shalloo, C. Arran, A. Picksley, A. von Boetticher, L. Corner, J. Holloway, G. Hine, J. Jonnerby, H. Milchberg, C. Thornton, R. Walczak, and S. Hooker, Physical Review Accelerators and Beams **22**, 041302 (2019).

[25] A. Picksley, A. Alejo, J. Cowley, N. Bourgeois, L. Corner, L. Feder, J. Holloway, H. Jones, J. Jonnerby, H. Milchberg, L. Reid, A. Ross, R. Walczak, and S. Hooker, Physical Review Accelerators and Beams **23**, 081303 (2020).

[26] A. Picksley, A. Alejo, R. J. Shalloo, C. Arran, A. von Boetticher, L. Corner, J. A. Holloway, J. Jonnerby, O. Jakobsson, C. Thornton, R. Walczak, and S. M. Hooker, Physical Review E **102**, 053201 (2020).

[27] A. Alejo, J. Cowley, A. Picksley, R. Walczak, and S. Hooker, Physical Review Accelerators and Beams **25**, 011301 (2022).

[28] J. Vieira, R. A. Fonseca, W. B. Mori, and L. O. Silva, Phys. Rev. Lett. **109**, 145005 (2012).

[29] R. D'Arcy, J. Chappell, J. Beinortaite, S. Diederichs, G. Boyle, B. Foster, M. J. Garland, P. G. Caminal, C. A. Lindstrøm, G. Loisch, S. Schreiber, S. Schröder, R. J. Shalloo, M. Thévenet, S. Wesch, M. Wing, and J. Osterhoff, Nature **603**, 58 (2022).

[30] R. Assmann, M. Weikum, and T. Akhter, European Physical Journal **4284**, 3675 (2019).

[31] B. Cros, P. Muggli, C. Schroeder, S. Hooker, P. Piot, J. England, S. Gessner, J. Vieira, E. Gschwendtner, J.-L. Vay, and M. Peskin, Arxiv (pre-print) (2019), 1901.10370.

[32] W. P. Leemans, R. Duarte, E. Esarey, S. Fournier, C. G. Geddes, D. Lockhart, C. B. Schroeder, C. Toth, J. L. Vay, and S. Zimmermann, AIP Conference Proceedings **1299**, 3 (2010).

[33] N. H. Matlis, S. Reed, S. S. Bulanov, V. Chvykov, G. Kalintchenko, T. Matsuoka, P. Rousseau, V. Yanovsky, A. Maksimchuk, S. Kalmykov, G. Shvets, and M. C. Downer, Nature Physics **2**, 749 (2006).

[34] N. Matlis, A. Maksimchuk, V. Yanovsky, W. Leemans, and M. Downer, Optics Letters **41**, 1 (2016).

[35] C. Arran, N. H. Matlis, R. Walczak, and S. M. Hooker, Physical Review Accelerators and Beams **21**, 1 (2018), 1810.06265.

[36] J. Derouillat, A. Beck, F. Pérez, T. Vinci, M. Chiaramello, A. Grassi, M. Flé, G. Bouchard, I. Plotnikov, N. Aunai, J. Dargent, C. Riconda, and M. Grech, Computer Physics Communications **222**, 351 (2018).

[37] A. Boetticher, S. Hooker, and R. Walczak, Submitted for publication (2022).

[38] J. R. Sanmartin, The Physics of Fluids **13**, 1533 (1970).